Check for updates

Research Article

INTERNATIONAL JOURNAL OF ADVANCED ROBOTIC SYSTEMS

International Journal of Advanced Robotic Systems
May-June 2021: 1–13
© The Author(s) 2021
Article reuse guidelines:
sagepub.com/journals-permissions
DOI: 10.1177/17298814211012325
journals.sagepub.com/home/arx
SAGE

A Novel 3-RRR Spherical Parallel Instrument for Daily Living Emulation (SPINDLE) for Functional Rehabilitation of Patients with Stroke

Peidong He[1], Nikhil Tej Kantu[1], Boxin Xu[1], Chinmay Prakash Swami[1], Ghazala T Saleem[2], and Jiyeon Kang[1,2]

Abstract

Various robotic rehabilitation devices have been developed for acute stroke patients to ease therapist's efforts and provide high-intensity training, which resulted in improved strength and functional recovery of patients; however, these improvements did not always transfer to the performance of activities of daily living (ADLs). This is because previous robotic training focuses on the proximal joints or training with exoskeleton-type devices, which do not reflect how humans interact with the environment. To improve the training effect of ADLs, a new robotic training paradigm is suggested with a parallel manipulator that mimics rotational ADL tasks. This study presents training of the proximal and distal joints simultaneously while performing manipulation tasks in a device named spherical parallel instrument for daily living emulation (SPINDLE). Six representative ADLs were chosen to show that both proximal and distal joints are trained when performing tasks with SPINDLE, as compared to the natural ADLs. These results show that SPINDLE can train individuals with movements similar to the ADLs while interacting with the manipulator. We envision using this compact tabletop device as a home-training device to increase the performance of ADLs by restoring the impaired motor function of stroke patients, leading to improved quality of life.

Keywords

Stroke rehabilitation, robotic rehabilitation, activities of daily living training, occupational therapy

Date received: 19 June 2020; accepted: 22 February 2021

Topic Area: Medical Robotics
Topic Editor: Alessandro Di Nuovo
Associate Editor: Giuseppe Carbone

Introduction

About 6.6 million individuals in the United States suffer from stroke-related motor impairments, and every year, about 800,000 individuals experience new or recurrent strokes.[1] Stroke patients often lose function of their upper limbs and have difficulty performing activities of daily living (ADLs). After the onset of stroke, the first 3 months is a crucial window when most of the rehabilitation happens by spontaneous neurological recovery.[2]

[1] Mechanical and Aerospace Engineering, University at Buffalo, Buffalo, NY, USA
[2] Rehabilitation Science, University at Buffalo, Buffalo, NY, USA

Corresponding author:
Jiyeon Kang, Mechanical and Aerospace Engineering, University at Buffalo, Buffalo, NY 14260, USA; Rehabilitation Science, University at Buffalo, 520 Lee Road, Furnas Hall, Room # 1011, Buffalo, NY 14228, USA.
Email: jiyeonk@buffalo.edu

Creative Commons CC BY: This article is distributed under the terms of the Creative Commons Attribution 4.0 License (https://creativecommons.org/licenses/by/4.0/) which permits any use, reproduction and distribution of the work without further permission provided the original work is attributed as specified on the SAGE and Open Access pages (https://us.sagepub.com/en-us/nam/open-access-at-sage).

During this acute stage, motor learning may help reduce motor impairment and facilitate recovery. The process of motor learning can be accelerated by rehabilitation, which may reduce chronic disabilities.[3] Occupational therapy (OT) services are often utilized to remediate or restore the function of the upper limbs. However, even after the completion of standard therapy, around 58% of individuals experience continuous challenges with ADLs.[4] Importantly, 4 years after the stroke incident, only 6% of patients are satisfied with the function of their impaired arm.[5] These residual impairments affecting ADLs indicate that OT may only have been moderately effective in improving ADLs outside of the hospital or clinic setting.[6,7] Stroke patients appear to often receive insufficient therapy for what is needed for effective rehabilitation.[8] Improvement of motor function for ADLs may occur through more intensive therapy.[9]

Robotic interventions have been developed in the past to satisfy high-intensity and repeated training. Many robotic interventions have been successful in improving upper limb motor scores and strength with devices such as MIT-Manus or Armeo Power,[10–13] but the consensus in literature demonstrates that these improvements do not always transfer to the performance of ADLs.[13] This may be due to the fact that these devices could have focused on the training of proximal joints, whereas integrating proximal with distal arm training may enhance functional gains needed for ADLs.[14,15] Second, many robotic interventions are focused on reaching tasks that are different from object manipulation. Many ADLs include manipulation tasks that require complicated three-dimensional (3D) hand posture changes. Third, robotic training sessions are often limited to patients in clinical settings because robotic systems are bulky and expensive, which make home-use challenging.

Various types of wrist rehabilitation robots have been developed to address this issue by training the distal arm. Earlier, wrist rehabilitation devices emphasized axial wrist rotation (pronation/supination) with an interface for stroke patients to practice grasping and wrist control.[16] Other exoskeleton-type designs with additional degrees of freedom (DoFs) were explored by adding wrist flexion/extension to the pronation/supination such as in Wrist Gimbal.[17] Furthermore, RiceWrist[18] employed three active DoFs with series elastic actuators to change the stiffness of the wrist joint during manipulation.

Soft robotic designs have also been developed for distal limb rehabilitation using cables and pneumatic actuators. CRAMER[19] and CDWRR[20] were developed featuring low-cost and lightweight cable-actuated mechanisms. However, these cable-actuated mechanisms showed high friction in their translational joints and low maneuverability during the wrist's fine motor control. Pneumatic actuator devices with a glove-type apparatus were developed for stroke patients as well,[21,22] adding wrist flexion/extension or radial/ulnar deviation.[23,24] These pneumatic designs have the benefit of being lightweight and having low inertia, resulting in higher safety from the compliance of the soft robotic structure. But these systems face issues with force/torque accuracy and are less compact due to the pneumatic system for actuation. Recent rigid exoskeleton-type devices for upper limb rehabilitation focus on having a higher range of motion, better manipulability, and higher torque performance.[25,26] Another new direction of wrist devices focuses on the compactness of the devices to develop lightweight systems stressing on the practical use of the devices.[27–30] Researchers tried to make the system more compact by implementing a compact series elastic actuator for variable stiffness control or employing smart mechanism for a fully portable 5-DoF wrist-elbow rehabilitation device.[29,30]

Most of the developed devices are exoskeleton type, which require aligning the human and robot joint axes before training the patient. These devices have the advantage of training the individual distal joints, but the training task is different from how humans use their upper limbs to interact with the environment. Exoskeleton-type devices control or apply forces on individual joints of the arm due to the alignment between its joint axis and human joint axis. This may lead to an increased burden on the patient as the device controls multiple joints simultaneously resulting in tight physical human–robot interaction.[31] In addition, a recent clinical study reported that the end-effector type of robotic training is more effective in Wolf Motor Function Test and Stroke Impact Scale scores, which represent the arm function related to the daily real-world activities.[31] Another study supports that robotic training is more efficient when combined with a transition-to-task OT, which indicates that the robotic intervention itself lacks the component to transfer the training effect to a real-world function.[32] Unlike other robotic designs that are built upon the human joint axis, the adaptive and automatic presentation of task (ADAPT) system was suggested to practice ADLs that require one-dimensional (1D) rotation of the tool. The tool was installed on a manipulator to change its orientation and height.[33] ADAPT is an innovative system with an emphasis on pieces of training similar to ADLs, but the tasks were limited only to a 1D rotation of the tool.

In this study, we propose a novel training strategy involving a rehabilitation robot named spherical parallel instrument for daily living emulation (SPINDLE). The design of the robot is inspired by the well-known agile eye structure, which is based on a 3-RRR parallel structure that enables 3D rotation.[34,35] This design allows for high stiffness, precise manipulation, and low inertia. Furthermore, it facilitates mimicking ADL tasks, which involve complicated manipulation of objects. The primary motivation behind the development of SPINDLE was to overcome some of the limitations of conventional OT and previous designs of rehabilitation robots, discussed earlier, to improve patients' performance on ADL tasks. SPINDLE will (i) enable training of both proximal and distal joints of the upper limb, which are crucial for performing ADL tasks.[14,15] Training regimes involving movement of all

3DoF of wrist can also be incorporated using SPINDLE; (ii) interact with the user as a human typically interacts with the environment in the real world. As this training resembles the real-world tasks, there is a higher chance of transferring the positive effects of training to real-world functions; (iii) allow for flexibility in movement unlike exoskeleton-type devices discussed earlier. This minimizes the burden of unnecessary human–robot interaction because this device does not require a nominal target trajectory for each individual joint of the upper limb[31]; (iv) enable training sessions to be carried out from home owing to its compact nature. Due to this, accessibility of the required therapy can be increased, a lack of which has been previously observed.[8] This compact nature will also enable high-intensity training, which has shown to improve performance in ADL tasks;[9] (v) allow for easier donning-doffing making it less time-consuming and less cumbersome compared to exoskeleton-type devices.

The rest of this article has the following structure: The design and structure of the suggested rehabilitation robot, SPINDLE, is presented in detail in the next section. Then, the optimization of design parameters and its result will be discussed in addition to the verification of the kinematic structure of SPINDLE. Following that, human testing will demonstrate SPINDLE as a training tool by presenting the usage of proximal and distal arm joints for six representative ADLs. The last part of this article presents the discussion and conclusion.

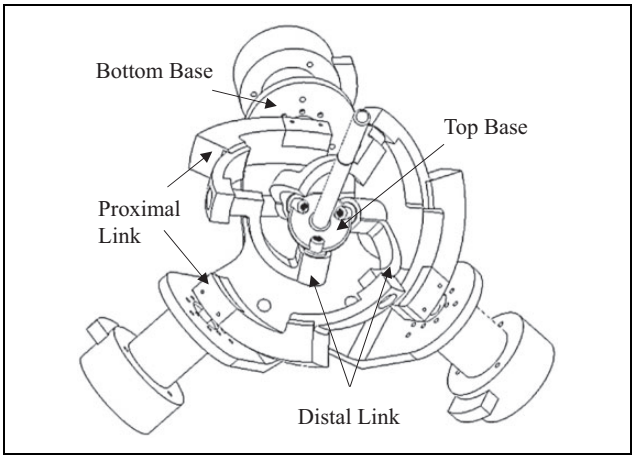


Figure 1. Architecture of proposed 3-RRR spherical parallel manipulator. Three motors actuate together to change the end-effector orientation.

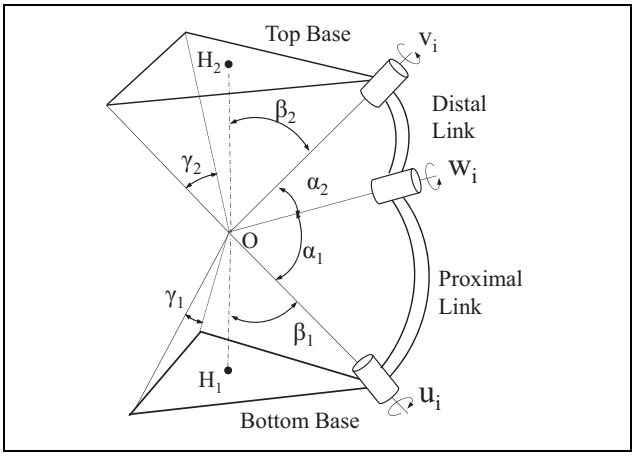


Figure 2. Schematic diagram of the 3-RRR spherical parallel manipulator. Each leg has three revolute joints: V_i on the top base, U_i on the bottom base, and W_i between the U_i and V_i.

Mathematical model of SPINDLE

Architecture of SPINDLE

Since the early 1980s, researchers have been broadly exploring the kinematic architecture of the spherical 3-RRR parallel manipulator due to its advantage of high stiffness and accuracy.[36–41] Motivated by the manipulator design in the previous study,[35] kinematic architecture shown in Figure 1 is chosen for training manipulation tasks during ADLs. The device employs 3-DoF rotation, which will allow the wrist to perform radial/ulnar deviation, flexion/extension, and pronation/supination. SPINDLE consists of three legs with three revolute joints and can create full-fledged three axial rotations in a large workspace. The patient will maneuver the top platform with a handle to generate 3D rotations to practice object manipulation tasks. The kinematic architecture of this structure is mathematically described with the following steps.

The manipulator consists of a top base and a bottom base connected by three curved isotropic legs, where each leg consists of three revolute joints in series. The center of the top base is indicated as H_2, and the center of the bottom base is indicated as H_1. This design minimizes the interference between linkages to utilize maximum workspace. The manipulator is designed to move along a spherical workspace with origin O. As shown in Figure 2, all revolute joints are designed to be located on the surface of the sphere and axes of these joints are perpendicular to the tangential plane on this spherical surface. Revolute joints at the movable top base are denoted as V_i ($i = 1, 2, 3$) of the i'th leg. U_i ($i = 1, 2, 3$) denotes revolute joints at the stationary bottom base, which are actuated by motors. The remaining revolute joints, placed between V_i and U_i, are denoted as W_i ($i = 1, 2, 3$). Rotating axes of joints U_i, V_i, and W_i are represented by unit vectors $\vec{u}_i$, $\vec{v}_i$, and $\vec{w}_i$. These vectors are all pointing from the sphere center O to the corresponding position of the rotational joint.

Two arc linkages are located between the rotational joints. Proximal link $L_{1,i}$ connects U_i and W_i joints at an angle α_1. Distal link $L_{2,i}$ connects V_i and W_i joints at an angle α_2. The arcs are concentric to the sphere center O. The design parameter γ_1 is defined as the angle between the unit vectors $\vec{u}_i$. Likewise, the design parameter γ_2 denotes the angle between unit vectors $\vec{v}_i$. The angle β_1

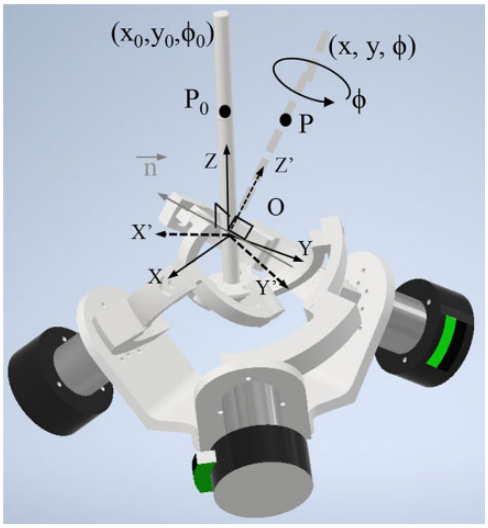


Figure 3. 3D CAD model of SPINDLE. The posture of the top base is denoted as a position (x, y) of a point P, which is the handle center and the rotation angle ϕ. SPINDLE: spherical parallel instrument for daily living emulation.

is located between the $\overline{OH}_1$ and the bottom base vectors $\vec{u}_i$. Furthermore, β_2 describes the angle between $\overline{OH}_2$ segments and the top base vectors $\vec{v}_i$. The global coordinate of XYZ is located in the sphere center O. The X–Y plane is defined to be parallel to the stationary bottom base, and Z axis is perpendicular to the bottom base. X axis is defined to be in the same plane as the first motor's rotational axis, $\vec{u}_1$.

Inverse kinematics

The inverse kinematics of the 3-RRR parallel manipulator is the foundation for motion control and trajectory planning. Prior to solving the inverse kinematics, it is crucial to first establish the home posture when all motor angles θ_i are zero. Home posture is defined when unit vectors $\vec{w}_i$ are located in the X–Y plane, which is parallel to the bottom base. The presented study uses intuitive notation of the end-effector posture instead of Euler angles to provide feedback to the patients on their training results. The posture of the end-effector is defined with the position (x, y) of the handle center P and the rotation angle (ϕ) around the center of the top base (Figure 3). The workspace of the parallel manipulator is composed of all points within a hemisphere that can be reached by the end-effector while rotating about itself from $-90°$ to $90°$.

For a given orientation of the handle (x, y, ϕ), the motor angles can be calculated by equation (1) using two rotational matrices (Q_2 and Q_1). The top base orientation can be defined by three unit vectors $\vec{v}_i$ with

$$\vec{v}_i = Q_2 Q_1 \vec{v}_{i0} \tag{1}$$

where $\vec{v}_{i0}$ is the vector $\vec{v}_i$ at the home posture. For computing a rotational matrix, a temporary variable Ψ is defined. Ψ represents the rotation angle between the global axis Z and the moving axis Z', as shown in Figure 3. Ψ is rotating along the axis $\vec{n} = \hat{Z} \times \hat{Z}'$. At the home posture, the local axis Z' is identical to the global axis Z. Q_1 is a rotation matrix calculated from the angle Ψ. Q_2 is a rotation matrix calculated with angle ϕ, which corresponds to the rotation around the local axis Z'. Matrices Q_1 and Q_2 yield

$$Q_1 = \begin{bmatrix} n_x^2 a + \cos\Psi, n_x n_y a - n_z \sin\Psi, n_x n_z a + n_y \sin\Psi \\ n_x n_y a + n_z \sin\Psi, n_y^2 a + \cos\Psi, n_y n_z a - n_x \sin\Psi \\ n_x n_z a - n_y \sin\Psi, n_y n_z a + n_x \sin\Psi, n_z^2 a + \cos\Psi \end{bmatrix} \tag{2}$$

$$Q_2 = \begin{bmatrix} x^2 b + \cos\phi, xyb - z\sin\phi, xzb + y\sin\phi \\ xyb + z\sin\phi, y^2 b + \cos\phi, yzb - x\sin\phi \\ xzb - y\sin\phi, yzb + x\sin\phi, z^2 b + \cos\phi \end{bmatrix} \tag{3}$$

where
$z = \sqrt{1 - x^2 - y^2}, a = 1 - \cos\Psi,$ and $b = 1 - \cos\phi$.

The next step is to define $\vec{w}_i$ with motor angles θ_i as

$$\vec{w}_i = \begin{bmatrix} c\alpha_1 c\eta_i s\beta_1 + (c\beta_1 c\eta_i s\theta_i - s\eta_i c\theta_i) s\alpha_1) \\ c\alpha_1 s\eta_i s\beta_1 + (c\beta_1 s\eta_i s\theta_i + c\eta_i c\theta_i) s\alpha_1) \\ -c\alpha_1 c\beta_1 + s\alpha_1 s\beta_1 s\theta_i \end{bmatrix} \tag{4}$$

where c indicates cos and s indicates sin. Then, $\vec{u}_i$ can be written with $\eta_i = 2(i-1)\pi/3$ as

$$\vec{u}_i = [\cos\eta_i \sin\beta_1, \sin\beta_1, -\cos\beta_1]^{\mathrm{T}} \tag{5}$$

By the definition of α_2, $\vec{w}_i$ and $\vec{v}_i$ are constrained as

$$\vec{w}_i \cdot \vec{v}_i = \cos\alpha_2 \tag{6}$$

Through equation (6), two solutions can be obtained. Considering all three legs of the parallel manipulator, there are three different sets of equations, which lead to eight possible solutions for a given end-effector posture. The solution nearest to the previous solution is chosen to avoid ambiguity.

Forward kinematics

The forward kinematics of a spherical surface manipulator has been well described by Gosselin et al.[34] The inputs of the forward kinematics are the angles of three electrical motors $(\theta_1, \theta_2, \theta_3)$ installed on the bottom base, while the output is the end-effector orientation (x, y, ϕ).

Let the end-effector orientation be expressed by three unit vectors, $\vec{v}_1, \vec{v}_2$, and $\vec{v}_3$. There are two design constraints that these vectors should satisfy. The first constraint is in equation (6) and the second constraint yields

$$\vec{v}_i \cdot \vec{v}_j = \cos\gamma_2, \qquad \text{where} \quad i \neq j \tag{7}$$

Using MATLAB fsolve function, multiple solutions satisfying equations (6) and (7) are identified. Similar to the inverse kinematics, the solution that is closest to the

previous solution is chosen. The forward kinematics is cross-verified with the inverse kinematics.

Jacobian

The moving platform rotates with a rotation vector ω. The motor is rotating with an angular speed $\dot{\theta}$, and the relative angular velocity of V_i respect to W_i is expressed as $\dot{\phi}$. A loop-closure equation can be written for each limb of the device

$$\overline{U_iV_i} = \overline{U_iO} + \overline{OV_i} \tag{8}$$

A velocity vector-loop equation is obtained by differentiating both sides of equation (8)

$$(\overline{OU_i} \cdot \overline{OV_i})\dot{\theta} + (\overline{OW_i} \times \overline{W_iV_i})\dot{\phi} = \overline{OV_i} \times \omega \tag{9}$$

Multiplication of both sides by $\overline{OW_i}$ cancels the passive angle $\dot{\phi}$, which leads to the following equation

$$(\overline{OW_i} \times \overline{OU_i} \cdot \overline{OV_i})\dot{\theta} = (\overline{OW_i} \times \overline{OV_i})\omega \tag{10}$$

Let

$$K_i \triangleq (\overline{OW_i} \times \overline{OU_i} \cdot \overline{OV_i}) \tag{11}$$

and

$$J_{k,i} \triangleq (\overline{OW_i} \times \overline{OV_i}), \tag{12}$$

The velocity equation for each leg of the spherical parallel manipulator can be written as $J_{k,i}\omega_i + K_i\dot{\theta}_i = 0$.[35] ω represents the angular velocity of moving platform and $\dot{\theta}_i$ is the angular velocity of i'th motor. Hence, the general velocity equation of the spherical parallel manipulator can be written as

$$J_k\omega + K\dot{\theta} = 0 \tag{13}$$

where $K = \mathrm{diag}(K_1, K_2, K_3)$ and $J_k = [J_{k1}, J_{k2}, J_{k3}]^{\mathrm{T}}$. Hence, the angular velocity of the moving platform can be obtained by the angular velocity of the motor through the Jacobian matrix, which can be written as

$$J = -J_k^{-1}K \tag{14}$$

Design parameter optimization

The range of the workspace depends on the design parameters α_1 and α_2. α_1 is the arc angle of $L_{1,i}$, which connects u_i and w_i. α_2 is the arc angle of $L_{2,i}$, which connects v_i and w_i. Design parameters α_1 and α_2 are determined to be 90° to obtain the maximum workspace.[42]

The design parameters γ_1 and γ_2 are chosen by two steps of optimization to maximize the controllability and the force transmitting efficiency of the manipulator. As the first step, a standard optimization method is used to evaluate the average kinematic performance of the whole workspace. The global conditioning index (GCI) by Gosselin and Angeles[43] is often employed to measure the kinematic performance, which is defined as

$$\mathrm{GCI} = \frac{\int_\Omega \frac{1}{\kappa}(J)\mathrm{d}w}{\int_\Omega \mathrm{d}w} = \frac{1}{W}\int_\Omega \frac{1}{\kappa}(J)\mathrm{d}w \tag{15}$$

where Ω represents the workspace of the manipulator. Condition number $\kappa(J)$ is defined as

$$\kappa(J) = \left\|J^{-1}\right\|\|J\| \tag{16}$$

where the norm of a matrix J is defined as

$$\|J\| = \sqrt{tr(J^TNJ)} \tag{17}$$

with $N = \frac{1}{3}I$ for the purpose of normalization. I is a 3×3 identity matrix. Based on the above equations, GCI can be written as[43]

$$\mathrm{GCI} = \frac{1}{W}\sum_{i=1}^{n}\frac{1}{\kappa_i}\Delta w_i \tag{18}$$

where n is the total number of discrete points and W is the volume of the workspace. The global maximum value of GCI is computed by dividing the hemispherical surface into discrete points with an interval of 10° in all directions.

The optimization result of GCI indicates that the optimal γ values are $\gamma_1 = 90°$ and $\gamma_2 = 74°$ with GCI = 0.7250. However, the value of GCI does not change much within the range of $\gamma_{1,\mathrm{GCI}} = 85° \sim 100°$ and $\gamma_{2,\mathrm{GCI}} = 70° \sim 90°$, as shown in Figure 4(a). This specific area is chosen for the second optimization to increase the force/torque transmission of the device. Unlike GCI, which evaluates the average kinematic performance, global minimum effective load (GMEL) compares only the points with the lowest transmitting efficiency for different γ_1 and γ_2. The hemisphere workspace of the parallel manipulator can be divided into 6840 different grid points to identify the lowest transmitting efficiency point. These grid points are created by dividing the workspace by 10° in the latitude/longitude directions and the axial rotation along the handle. If the force transmitting performance toward a specific direction in a specific point of the workspace is the lowest, it is defined as the minimum effective load. Maximizing the GMEL will mitigate the worst force transmitting efficiency of the manipulator. GMEL for the given design parameters γ_1 and γ_2 can be defined as

$$\mathrm{GMEL} = \min\varepsilon, \qquad \text{where} \quad \varepsilon \in E \tag{19}$$

where ε indicates the transmission performance of a specific posture and $E = \{\varepsilon | \forall(x, y, \phi) \in W\}$. ε is defined as

$$\varepsilon = \min\frac{\left|J^T\vec{f}\right|}{\tau_{\max}}, \qquad \text{where} \quad \vec{f} \in F \tag{20}$$

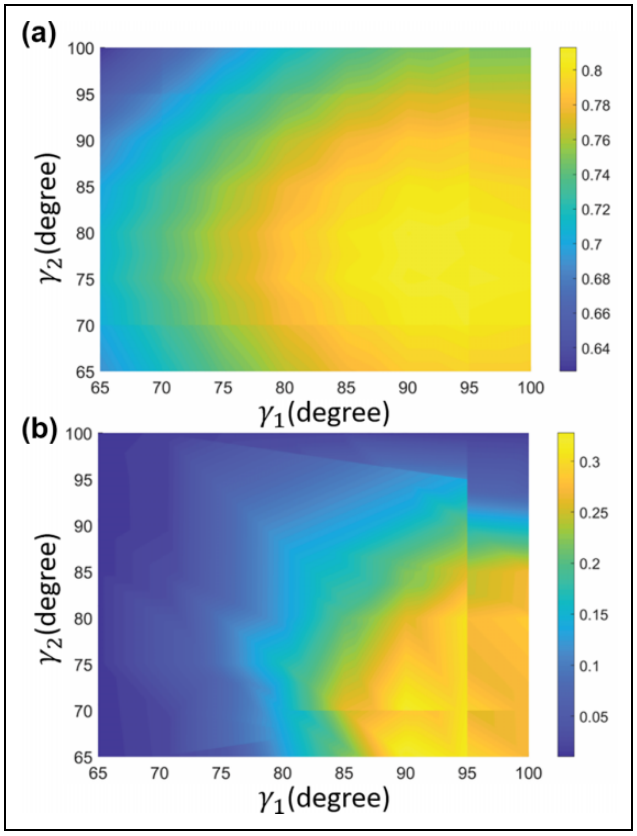


Figure 4. Results of design parameter optimization with respect to angles γ_1 and γ_2. (a) GCI and (b) global minimum effective load results. GCI: global conditioning index; GMEL: global minimum effective load.

where $\vec{f}$ is a unit vector representing the direction of the force generated at the end-effector. F represents the set of unit force vectors in all 3D directions for a given point. $\tau_{\max}$ is the rated maximum torque value of the motor. Optimization of GMEL determines $\gamma_{1,\mathrm{GMEL}} = 90^\circ$ and $\gamma_{2,\mathrm{GMEL}} = 72^\circ$ with $\mathrm{GMEL}_{\max} = 0.3179$ (Figure 4(b)). When these parameters are used, GCI value does not change much, when compared to the optimal GCI value. Optimal GCI value is $\mathrm{GCI}_{\max} = 0.7250$, but GCI value of the optimal GMEL is $\mathrm{GCI}_{\mathrm{GME}} = 0.7170$.

Device set-up

Physical device

A rehabilitation device for stroke patients is designed as a 3-RRR parallel manipulator, which is capable of 3D rotational movements (Figure 5). Three legs of the manipulator connect a bottom base and a top base of the parallel manipulator. Motors with an encoder are installed on the bottom base of the manipulator to actuate these legs.

The manipulator can provide nearly 180° of rotation in all three axes. The row, pitch, and yaw movements are shown in Figure 5. The manipulator is controlled by three

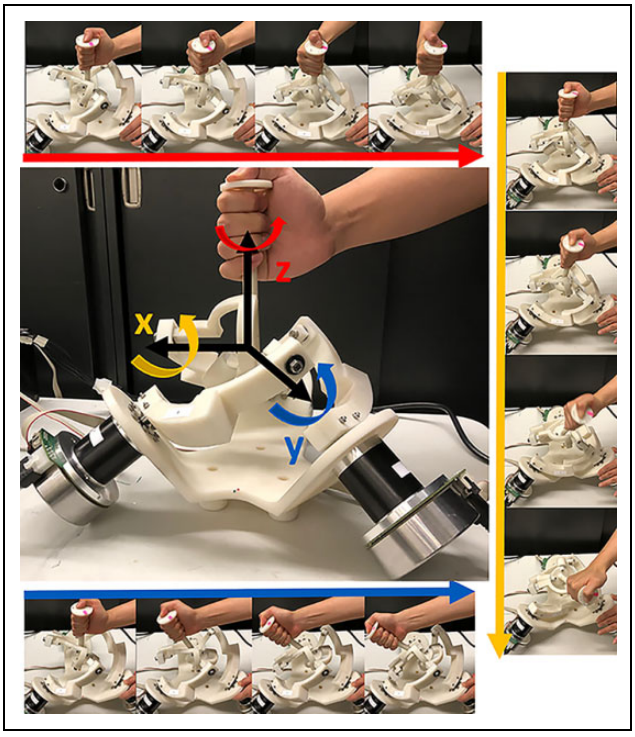


Figure 5. Prototype of the spherical parallel instrument for daily living emulation (SPINDLE). Different configurations of SPINDLE showing (right) roll (top) yaw (bottom) pitch manipulation. SPINDLE: spherical parallel instrument for daily living emulation.

EC 90 flat motors (Maxon Inc., Switzerland), which are powered by three ESCON 70/10 controller (Maxon Inc.). An amplitude of -90° to 90° can be achieved along X, Y, and Z axes with maximum torques of 7.34, 7.54, and 8.15 Nm, respectively. The dimensions of the SPINDLE are 427 mm (H) × 400 mm (W) × 348 mm (L) and it weighs about 4.5 kg. This system operates under the command of a remote control PC to myRIO 1900 (National Instrument Inc., Texas, USA) at a frequency of 500 Hz. The linkages of SPINDLE are made with tough resin material from a 3D printer to endure high stress and strain.

Verification of kinematic structure of SPINDLE

A motion capture system with 10 optical cameras (Vicon, UK) operating at 100 Hz was used to compare the kinematics of the mathematical model and physical device. There were 11 reflective markers attached on each part of SPINDLE. Four markers were on the handle to obtain the Z' axis, three markers were on the top base, and four markers were on the bottom base. Before capturing the motion of the device, the device was set in the home posture. The top base was adjusted to be parallel with the ground, and the motor angles were set to zero. When the user moved the end-effector, a new position $P(x, y, \phi)$ was computed by two steps. The position (x, y) was computed from two markers placed at the position P. The angle ϕ was computed from three markers on the top base rotating

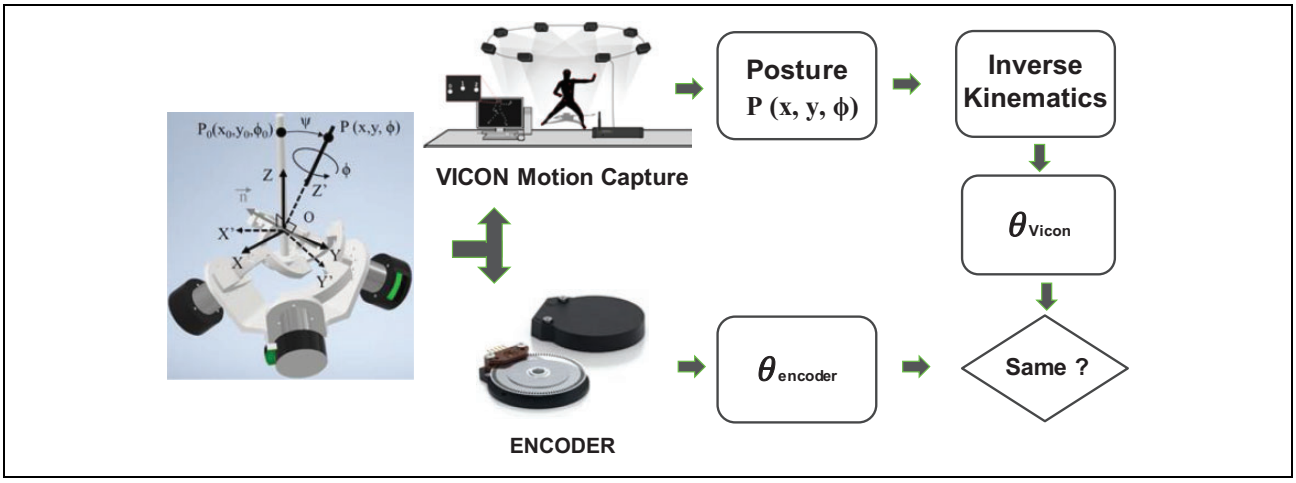


Figure 6. Schematic to compare the joint angles $\theta_{\text{Vicon},i}$ and $\theta_{\text{Encoder},i}$. $\theta_{\text{Vicon},i}$ is computed from a motion capture system and $\theta_{\text{Encoder},i}$ is computed from encoders.

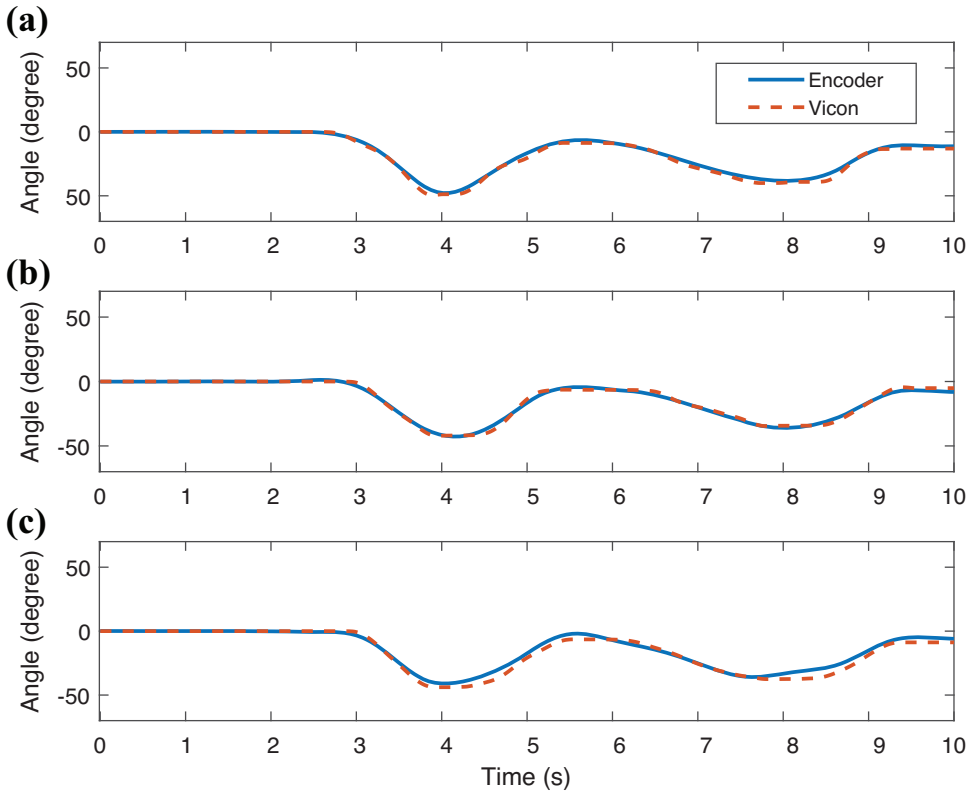


Figure 7. Comparison of angle values recorded by motor encoders and motion capture system. (a–c) The top, middle, and bottom diagrams represent the angles of motors 1, 2, and 3, respectively.

along the axis Z' after the axis Z' was computed by markers on the handle.

The inverse kinematics of SPINDLE is used to calculate angles of the joints U_i with respect to the posture of the top base (x, y, ϕ), as shown in Figure 6. The joint angle $\theta_{\text{Encoder},i}$ is computed from the encoder and the joint angle $\theta_{\text{Vicon},i}$ is computed from motion capture system for $i = 1, 2, 3$. During the motion capture, each encoder recorded the rotation angles of the motor. Figure 7 shows the motor angles recorded from the encoders and computed from the end-effector posture using inverse kinematics. The root mean square error values of motor angles during 10 s are $\theta_1 = 1.877°$, $\theta_2 = 1.446°$, and $\theta_3 = 3.066°$.

Feasibility human experiment for activities of daily living

Six example tasks performed on SPINDLE

To show the feasibility of training ADL tasks on SPINDLE, six representative tasks were designed, as shown in Figure 8. Six ADL tasks were chosen to demonstrate the training of both proximal and distal joints during object manipulation. The upper limb movement during the task was recorded by a motion capture system. The participant was blinded for the study and repeated each task for 10 trials. The inclusion criterion for the study required the participants (18–65 years old) to be healthy and fit to perform active daily living tasks. Individuals with upper limb prosthetics, loss of sensation, uncontrolled blood pressure, seizure disorder, severe arthritis, or other upper extremity orthopedic conditions that limit their activity level were excluded from this study.

The first task was to open and close a jar cap (jar), and the second task was to stir a pot with a ladle (ladle). This task started when the participant naturally held the ladle in hand and aligned the ladle with medial–lateral direction of the participant. The participant performed stirring action in the counterclockwise direction. The third task was to empty the water from a pitcher (pitcher). The participant started at the default position by holding the pitcher vertically. The participant mimicked emptying the water from the pitcher into a cup and was asked to be consistent with the height of the hand when holding the pitcher. The fourth task was to open and close a book (book). The fifth task was designed to mimic pouring water from a cup (cup). The cup task started while holding the cup vertically and performing pouring movements. Finally, the sixth task was to tighten and loosen a screw with a screwdriver (screwdriver). The default position of the screwdriver was 90° with the screw holder. Ten trials were performed for each task. After the completion of six tasks, the participant was asked to perform the same tasks on SPINDLE with similar instructions.

Comparison of upper limb angles measured from ADLs and SPINDLE

To understand the kinematic nature of ADL and SPINDLE training, 19 markers were attached to the upper body of a healthy participant. Markers were placed on the following positions to compute the ZYX Euler angles of the shoulder, elbow, and wrist: seventh cervical vertebrae, eighth thoracic vertebrae, sternum for the trunk; acromion, deltoid, lateral epicondyle of the humerus, medial epicondyle of the humerus, radial styloid, ulnar styloid, third metacarpal bone, mid-humerus, mid-radial, and mid-ulnar for the upper arm. The local axes to compute Euler angles were attached to the center of the joint. The local x-axis was set to be the flexion/extension axis of the joint and the local y-axis was set to be approximately in the direction of the segment of the upper limb. As shown in Figure 8, the Euler angles are presented for each joint of the upper limb along z, y, and x axes, which are indicated as α, β, and γ, respectively.

For each trial, the minimum and maximum values of Euler angles during the tasks were computed. The average and standard deviation of nine trials were computed, as presented in Table 1 for six different tasks. To compare the actual task and SPINDLE, a one-way multivariate analysis of variance (MANOVA) was performed because this study includes multiple sample means between the actual and SPINDLE tasks, such as shoulder, elbow, and wrist Euler angles. MANOVA was performed for each task using statistics software SPSS (IBM Inc,. Illinois, USA) with shoulder, elbow, and wrist Euler angles as dependent variables.[44]

MANOVA was performed individually for each task to verify the significant differences between task types (natural vs. SPINDLE). For the book task, MANOVA showed that all participants reported no statistically significant differences in all Euler angles between natural and SPINDLE tasks ($p_{\text{Ladle},1} = 0.057, p_{\text{Ladle},2} = 0.075, p_{\text{Ladle},3} = 0.065$.) The screw and book tasks showed no significant differences except subject 3: $p_{\text{Screw},1} = 0.249$, $p_{\text{Screw},2} = 0.132$, $p_{\text{Screw},3} = 0.048$, $p_{\text{Book},1} = 0.079$, $p_{\text{Book},2} = 0.062$, $p_{\text{Book},3} = 0.025$. The jar task showed no significant difference in subject 3: $p_{\text{Jar},1} = 0.035$, $p_{\text{Jar},2} = 0.016$, $p_{\text{Jar},3} = 0.091$, the cup and pitcher tasks showed significant differences in all participants: $p_{\text{Cup},1} = 0.000$, $p_{\text{Cup},2} = 0.013$, $p_{\text{Cup},3} = 0.020$, $p_{\text{Pitcher},1} = 0.000$, $p_{\text{Pitcher},2} = 0.024$, $p_{\text{Pitcher},3} = 0.002$. The significant differences were observed when the movement of the object did not have any constraints and the object was lightweight. Presumably, the user performed the task differently with SPINDLE due to the movement constraint that is created by the structure of SPINDLE. Even though they show significant difference, it should be noted that the angle values were similar in both SPINDLE and natural tasks. For example, for the pitcher task, Table 1 presents that the angles in the pitcher task were only a few degrees difference between the natural and SPINDLE tasks.

Discussion and future work

This study presents a 3D rotational knob, SPINDLE, suggesting a rehabilitation strategy to let the user experience delicate rotational movements that are similar to ADL tasks. Particularly, this study shows the kinematic structure and the feasibility of SPINDLE as a training tool. Six representative ADL tasks were chosen to show that SPINDLE can train both proximal and distal joints of the limb with a range of motion similar to natural ADL tasks. The device features a wide range of motion and high torque capability compared to off-the-shelf haptic devices. Using mathematical models and encoder data, the device can serve as a

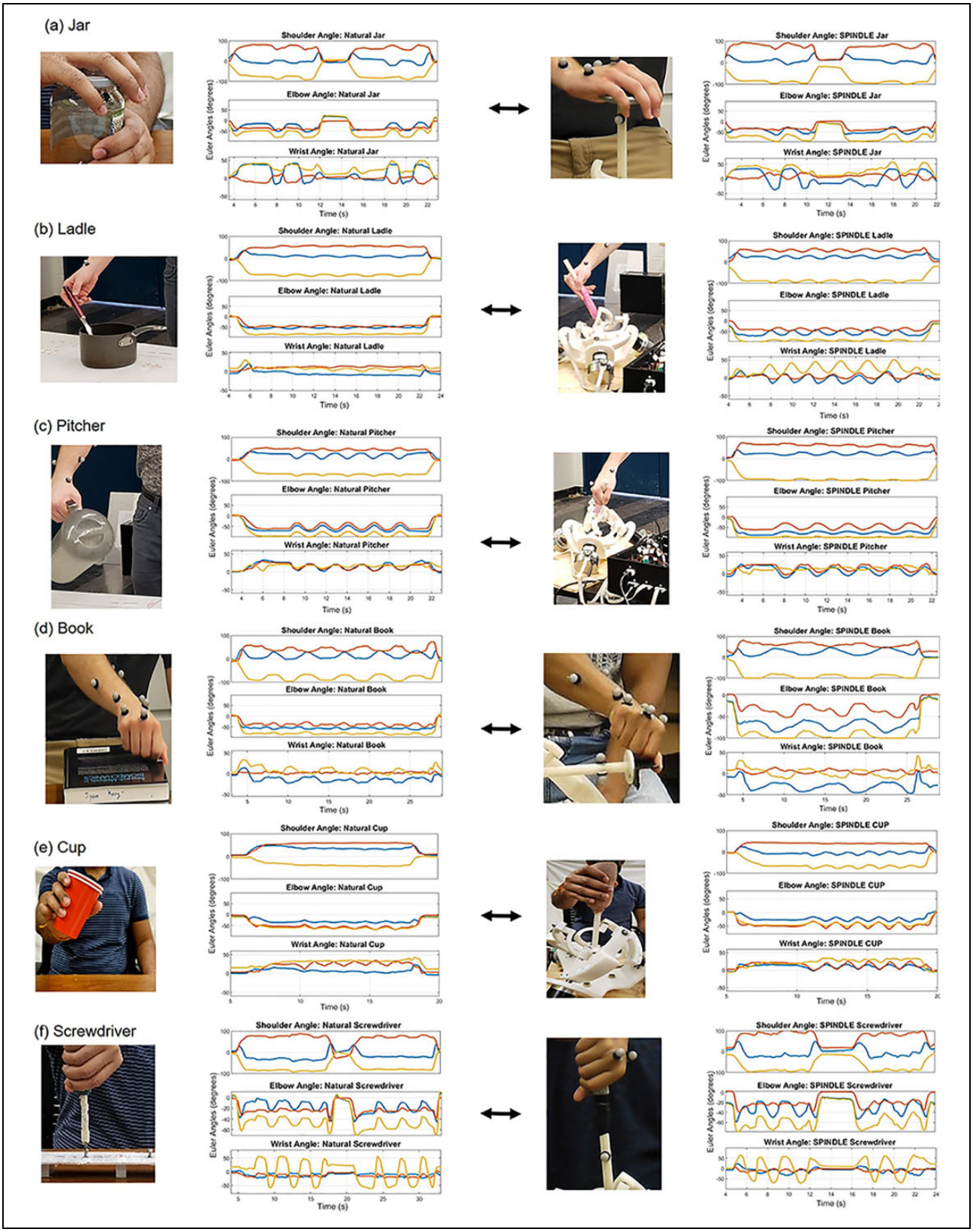


Figure 8. Movement comparison of natural and SPINDLE tasks during activities of daily living: (a) opening and closing a jar cap, (b) stirring a ladle to mix a pot, (c) pouring water from a pitcher, (d) flipping a book, (e) pouring water from a cup, (f) using a screwdriver to tighten and loosen a screw. Euler angles are computed for *ZYX* Euler convention for α (blue), β (orange), and γ (yellow). SPINDLE: spherical parallel instrument for daily living emulation.

Table 1. Comparisons of upper limb joint angles for natural and SPINDLE tasks for six representative activities during daily living ($N = 3$).

	Task type	Natural						SPINDLE					
Task	Joint	α_{min}	α_{max}	β_{min}	β_{max}	γ_{min}	γ_{max}	α_{min}	α_{max}	β_{min}	β_{max}	γ_{min}	γ_{max}
Jar	Shoulder	−22.96	86.44	−10.23	71.51	−66.59	35.57	−23.52	85.12	−6.03	75.57	−65.76	35.22
	Elbow	−46.59	11.73	−52.58	1.61	−72.11	12.90	−44.87	11.19	−50.40	3.74	−69.46	10.93
	Wrist	−18.06	42.82	−16.83	9.69	5.68	49.73	−30.99	39.29	−11.10	20.25	−2.95	49.05
Ladle	Shoulder	−5.21	59.19	−6.26	59.61	−60.23	14.16	−9.28	71.41	1.42	58.51	−58.95	18.52
	Elbow	−46.96	3.56	−51.31	0.06	−73.75	0.88	−51.31	1.73	−51.22	0.84	−74.38	−1.13
	Wrist	−9.68	12.87	−1.94	20.46	−2.28	25.81	−7.59	21.36	−5.71	25.09	−5.67	42.71
Pitcher	Shoulder	−4.40	61.68	−5.97	53.75	−54.82	11.47	−9.39	68.15	−8.82	62.43	−68.82	17.87
	Elbow	−60.19	0.39	−61.90	0.30	−85.00	0.24	−59.63	3.10	−58.55	9.91	−79.21	9.20
	Wrist	−3.70	31.34	−1.73	29.80	6.58	39.34	−10.18	26.05	−1.07	33.49	−8.41	25.80
Book	Shoulder	−10.09	65.89	−5.26	59.32	−66.50	16.61	−13.81	75.05	−3.36	63.70	−64.82	31.35
	Elbow	−58.97	2.12	−53.28	0.20	−78.74	−1.08	−63.39	5.06	−49.13	3.63	−75.25	4.04
	Wrist	−21.45	12.37	−4.94	22.65	−6.09	28.75	−37.85	11.66	−5.70	19.44	−3.80	28.19
Cup	Shoulder	−5.74	63.38	−4.12	55.66	−40.91	6.98	−5.20	73.03	−2.62	60.44	−60.12	14.67
	Elbow	−58.84	0.14	−70.53	0.67	−88.70	−0.63	−61.77	0.62	−69.72	3.50	−82.52	−0.27
	Wrist	5.64	31.47	0.32	34.82	6.87	42.68	−7.03	23.27	−0.23	34.44	2.07	41.99
Screwdriver	Shoulder	−27.92	97.27	−10.08	72.78	−61.62	54.80	−45.12	101.33	−0.39	81.69	−72.94	60.68
	Elbow	−39.17	10.17	−47.81	1.06	−61.72	2.53	−30.75	22.13	−36.77	10.42	−57.98	11.61
	Wrist	−22.90	7.41	−26.65	8.46	−56.14	60.36	−29.49	23.73	−25.82	12.62	−63.86	77.14

measurement tool for quantifying the manipulation capability of patients with acute stroke by computing the range of motion from the end-effector rotation.

The device can address multiple issues of conventional OT and previous robotic intervention to enhance the performance of ADLs in stroke patients. First, stroke patients appear to receive only a small dosage of the needed therapy for effective rehabilitation.[8] SPINDLE is a tabletop device that has the potential to be installed at home due to its compact nature. Easier access to the training will increase the training time of patients with acute stroke. Second, the clinical assessments to measure the efficacy of OT appear to be coarse and insufficient. Due to the diversity of tasks used during therapy, quantification of the efficacy of OT has been challenging and has shown only moderate results to enhance the performance of ADLs. The current measures to evaluate the performance of OT interventions are the Barthel index, the Fugl Meyer, and the Nottingham extended activities of daily living, which are all descriptive and subjective.[45,46] SPINDLE can provide systematic quantification of task performance and manipulation capability of the patient. Immediate performance feedback to the patients can also positively influence participants' motivation and self-efficacy.[47–49] Third, the current robotic intervention has shown moderate results on the enhancement of ADLs. This may be due to the fact that these devices could have focused on the training of proximal joints, whereas integrating proximal with distal arm training may enhance functional gains needed for ADLs.[14,15] Six representative tasks showed thst SPINDLE can train both distal and proximal joints, which also enable practicing tasks of manipulating objects.

The errors of the kinematic verification might have been generated due to three possible reasons. First, the home position could not be set precisely during the calibration. The kinematics is computed based on the home posture, which could create bias of motor angles when computing inverse kinematics. Secondly, the backlash of the motor could create inaccurate measures of the motor angle when recording the movement of the end-effector. Lastly, markers used to identify the orientation and the position of the end-effector could not have been attached in an accurate position.

Future work will focus on different parts. First, the task movement between SPINDLE and the actual ADLs will be further studied. The current study presents only minimum and maximum values for comparison. Other factors such as smoothness, speed, and travel distance of the movement will be explored. Second, the implementation of an admittance controller to mimic the physical characteristics of different objects will be the main focus. An ATI Mini 45 (ATI Industrial Automation, North Carolina, USA), a six-axis force/torque sensor, will be installed on the handle to measure the human-interaction force and the data will be used to mimic the physical characteristics of virtual objects by electrical motors. These motors will render the virtual admittance that will be assigned by a physical or occupational therapist depending on the patient's strength and motor control ability. Third, a virtual reality system will make the manipulator visually realistic. A virtual reality goggle will show a familiar object that is used frequently in daily activities. The wireless Vive Pro (HTC, Taiwan) will be used to create a virtual object and match it with the motion of SPINDLE using encoder values. In addition,

exploration of different methods will provide proper visual feedback related to their performance during the task. New strategies to teach the SPINDLE how to train the patients by learning from occupational therapists will be also explored in the near future.[50,51] Lastly, acute stroke patients will be recruited by the team to show the feasibility of the intervention with SPINDLE. The target population will be stroke patients who have minimal strength to move their arm and have difficulties in performing dexterous manipulations.

Conclusion

We present a feasibility study to use a 3-RRR parallel manipulator, named SPINDLE, for training ADLs of stroke patients. The inverse kinematics, forward kinematics, and the Jacobian matrix of the SPINDLE are derived, and the design parameters are optimized to maximize the workspace and the control performance of SPINDLE. The physical device is introduced with a verification of the mathematical model using a motion capture system. The study shows six representative ADLs that were performed both on SPINDLE and the actual task. The experimental results show that SPINDLE can train both proximal and distal joints, which are essential for independently carrying out ADLs. Also, the upper limb joint movements are similar between the natural and SPINDLE tasks. SPINDLE can train the user in a way similar to how humans interact with their environment. This compact tabletop device could be installed in ICUs, homes, or community centers to train the upper limb of stroke patients for enhancing their ADL performance and quality of life.

The limitation of this work is that only three healthy participants were included in the study. In the future, more participants will be recruited, including stroke patients to show the efficacy of the presented training method. For stroke patients, the human–robot interface should also be further investigated to secure the hand of the stroke patients on the robot. We are also planning to use an elbow rest in case the participant is too weak to hold the arm against gravity. Future work will focus on the hypothesis-driven studies with stroke patients to verify whether the training from the ADL tasks on SPINDLE can transfer to actual real-world tasks by evaluating their daily activities using Barthel index or functional ability rating scale.

Acknowledgements

The authors thank Nicholas Lenhard for helping to collect and analyze the joint angle data.

Declaration of conflicting interests

The author(s) declared no potential conflicts of interest with respect to the research, authorship, and/or publication of this article.

Funding

The author(s) received no financial support for the research, authorship, and/or publication of this article.

ORCID iDs

Chinmay Prakash Swami https://orcid.org/0000-0002-8200-8481

Jiyeon Kang https://orcid.org/0000-0003-4154-8593

References

1. Benjamin EJ, Blaha MJ, Chiuve SE, et al. Heart disease and stroke statistics-2017 update: a report from the American Heart Association. *Circulation* 2017; 135(10): e146–e603.
2. Dobkin BH. Rehabilitation after stroke. *N Eng J Med* 2005; 94(3–4): 1677–1684.
3. Duncan P, Studenski S, Richards L, et al. Randomized clinical trial of therapeutic exercise in subacute stroke. *Stroke* 2003; 34(9): 2173–2180.
4. Sturm JW, Dewey HM, Donnan GA, et al. Handicap after stroke: how does it relate to disability, perception of recovery, and stroke subtype? the north east Melbourne stroke incidence study (NEMESIS). *Stroke* 2002; 33(3): 762–768.
5. Broeks J, Lankhorst G, Rumping K, et al. The long-term outcome of arm function after stroke: results of a follow-up study. *Disabil Rehabil* 1999; 21(8): 357–364.
6. Doman CA, Waddell KJ, Bailey RR, et al. Changes in upper-extremity functional capacity and daily performance during outpatient occupational therapy for people with stroke. *Am J Occup Ther* 2016; 70(3): 1–11.
7. Waddell KJ, Strube MJ, Bailey RR, et al. Does task- specific training improve upper limb performance in daily life post-stroke? *Neurorehabil Neural Repair* 2017; 31(3): 290–300.
8. Lang CE, MacDonald JR, Reisman DS, et al. Observation of amounts of movement practice provided during stroke rehabilitation. *Arch Phys Med Rehabil* 2009; 90(10): 1692–1698.
9. Kwakkel G. Intensity of practice after stroke: more is better. *Schweizer Archiv fur Neurologie und Psychiatrie* 2009; 160(7): 295–298.
10. Mehrholz J, Häädrich A, Platz T, et al. Electromechanical and robot-assisted arm training for improving generic activities of daily living, arm function, and arm muscle strength after stroke. *Cochrane Database Syst Rev* 2012; 4(6): CD006876.
11. Prange G, Jannink M, Groothuis-Oudshoorn C, et al. Systematic review of the effect of robot-aided therapy on recovery of the hemiparetic arm after stroke. *J Rehabil Res Dev* 2009; 43(2): 171–184.
12. Lo AC, Guarino PD, Richards LG, et al. Robot-assisted therapy for long-term upper-limb impairment after stroke. *N Eng J Med* 2010; 362(19): 1772–1783.
13. Kwakkel G, Kollen BJ, and Krebs HI. Effects of robot-assisted therapy on upper limb recovery after stroke: a systematic review. *Neurorehabil Neural Repair* 2008; 22(2): 111–121.
14. Oujamaa L, Relave I, Froger J, et al. Rehabilitation of arm function after stroke. Literature review. *Ann Phys Rehabil Med* 2009; 52(3): 269–293.

15. Timmermans AA, Seelen HA, Willmann RD, et al. Technology- assisted training of arm-hand skills in stroke: concepts on reacquisition of motor control and therapist guidelines for rehabilitation technology design. *J Neuroeng Rehabil* 2009; 6(1): 1.
16. Lambercy O, Dovat L, Gassert R, et al. A haptic knob for rehabilitation of hand function. *IEEE Trans Neural Syst Rehabil Eng* 2007; 15(3): 356–366.
17. Saadatzi M, Long DC, and Celik O. Comparison of human-robot interaction torque estimation methods in a wrist rehabilitation exoskeleton. *J Intell Robot Syst* 2019; 94: 565–581.
18. Pehlivan AU, Sergi F, Erwin A, et al. Design and validation of the RiceWrist-S exoskeleton for robotic rehabilitation after incomplete spinal cord injury. *Robotica* 2014; 32(8): 1415–1431.
19. Spencer SJ, Klein J, Minakata K, et al. A low cost parallel robot and trajectory optimization method for wrist and forearm rehabilitation using the Wii. In: *2008 2nd IEEE RAS & EMBS international conference on biomedical robotics and biomechatronics*, Scottsdale, AZ, USA, 19–22 October 2008, pp. 869–874. IEEE.
20. Cui X, Chen W, Agrawal SK, et al. A novel customized Cable- driven robot for 3-DOF wrist and forearm motion training. In: *2014 IEEE/RSJ international conference on intelligent robots and systems*, Chicago, IL, USA, 14–18 September 2014, pp. 3579–3584. IEEE.
21. Yurkewich A, Hebert D, Wang RH, et al. Hand extension robot orthosis (HERO) glove: development and testing with stroke survivors with severe hand impairment. *IEEE Trans Neural Syst Rehabil Eng* 2019; 27(5): 916–926.
22. Heung KHL, Tong RKY, Lau ATH, et al. Robotic glove with soft-elastic composite actuators for assisting activities of daily living. *Soft Robot* 2019; 6(2): 289–304.
23. Ang BWK and Yeow C-H.Design and characterization of a 3D printed soft robotic wrist sleeve with 2 DoF for stroke rehabilitation. In: *2019 2nd IEEE international conference on soft robotics (RoboSoft)*, Seoul, Korea (South), 14–18 April 2019, pp. 577–582. IEEE.
24. Zhang L, Li J, Cui Y, et al. Design and performance analysis of a parallel wrist rehabilitation robot (PWRR). *Robot Autonom Syst* 2020; 125: 103390.
25. Zimmermann Y, Forino A, Riener R, et al. ANYexo: a versatile and dynamic upper-limb rehabilitation robot. *IEEE Robot Autom Lett* 2019; 4(4): 3649–3656.
26. Lee J, Song B, and Yang W. ANYexo design of exoskeleton-type wrist human–machine interface based on over-actuated coaxial spherical parallel mechanism. *Adv Mech Eng* 2018; 10(2): 1687814017753896.
27. Cafolla D, Russo M, and Carbone G. CUBE, a cable-driven device for limb rehabilitation. *J Bionic Eng* 2019; 16(3): 492–502.
28. Carbone G, Cavero CA, Ceccarelli M, et al. A study of feasibility for a limb exercising device. In: Boschetti G and Gasparetto A (eds) *Advances in italian mechanism science*. Cham: Springer, 2017, pp. 11–21.
29. Zhang Q, Sun D, Qian W, et al. Modeling and control of a cable-driven rotary series elastic actuator for an upper limb rehabilitation robot. *Front Neurorobot* 2020; 14: 13.
30. Wu K, Su Y, Yu Y, et al. A 5-degrees-of-freedom lightweight elbow-wrist exoskeleton for forearm fine-motion rehabilitation. *IEEE/ASME Trans Mechatron* 2019; 24(6): 2684–2695.
31. Lee S H, Park G, Cho D Y, et al. Comparisons between end-effector and exoskeleton rehabilitation robots regarding upper extremity function among chronic stroke patients with moderate-to-severe upper limb impairment. *Sci Rep* 2020; 10(1): 1–8.
32. Conroy SS, Wittenberg GF, Krebs HI, et al. Robot-assisted arm training in chronic stroke: addition of transition-to-task practice. *Neurorehabil Neural Repair* 2019; 33(9): 751–761.
33. Choi Y, Gordon J, Kim D, et al. An adaptive automated robotic task-practice system for rehabilitation of arm functions after stroke. *IEEE Trans Robot* 2009; 25(3): 556–568.
34. Gosselin C, Sefrioui J, and Richard MJ. On the direct kinematics of spherical three-degree-of-freedom parallel manipulators with a coplanar platform. *J Mech Des* 1994; 116(2): 587–593.
35. Gosselin CM, Pierre ES, and Gagne M. On the development of the agile eye. *IEEE Robot Autom Mag* 1996; 3(4): 29–37.
36. Asada H and Youcef-Toumi K. Analysis and design of a direct-drive arm with a five-bar-link parallel drive mechanism. *J Dyn Syst Meas Control* 1984; 106(3): 225–230.
37. Asada H and Ro IH. A linkage design for direct-drive robot arms. *J Mech Transm Autom Des* 1985; 107(4): 536–540.
38. Bajpai A and Roth B. Workspace and mobility of a closed-loop manipulator. *Int J Robot Res* 1986; 5(2): 131–142.
39. Hunt K. Structural kinematics of in-parallel-actuated robot arms. *J Mech Des* 1983; 105(4): 705–712.
40. Yang D and Lee T. Feasibility study of a platform type of robotic manipulators from a kinematic viewpoint. *J Mech Trans Autom Des* 1984; 106(2): 191–198.
41. Mohamed M and Duffy J. A direct determination of the instantaneous kinematics of fully parallel robot manipulators. *J Mech Des* 1985; 107(2): 226–229.
42. Gosselin C and Angeles J. The optimum kinematic design of a spherical three-degree-of-freedom parallel manipulator. *J Mech Des* 1989; 111(2): 202–207.
43. Gosselin C and Angeles J. A global performance index for the kinematic optimization of robotic manipulators. *J Mech Des* 1991; 113(3): 220–226.
44. Zar J. *Biostatistical analysis*. 5th ed. New York, NY: Pearson Press, 1998.
45. Mahoney FI and Barthel DW. Functional evaluation: the Barthel index: a simple index of independence useful in scoring improvement in the rehabilitation of the chronically ill. *Md State Med J* 1965; 14: 61–65.
46. Nouri F and Lincoln N. An extended activities of daily living scale for stroke patients. *Clin Rehabil* 1987; 1(4): 301–305.
47. Annesi JJ. Effects of computer feedback on adherence to exercise. *Percept Mot Skills* 1998; 87(2): 723–730.

48. Jones F. Strategies to enhance chronic disease self-management: how can we apply this to stroke? *Disabil Rehabil* 2006; 28(13–14): 841–847.
49. Van Vliet PM and Wulf G. Extrinsic feedback for motor learning after stroke: what is the evidence? *Disabil Rehabil* 2006; 28(13–14): 831–840.
50. Su H, Qi W, Hu Y, et al. An incremental learning framework for human-like redundancy optimization of anthropomorphic manipulators. *IEEE Trans Ind Inform* 2020: 1–1.
51. Su H, Mariani A, Ovur SE, et al. Toward teaching by demonstration for robot- assisted minimally invasive surgery. *IEEE Trans Autom Sci Eng* 2021; 18: 484–494.